HHS Public Access

Author manuscript

J Nucl Med. Author manuscript; available in PMC 2016 October 01.

Published in final edited form as:

J Nucl Med. 2015 October ; 56(10): 1587–1592. doi:10.2967/jnumed.115.160754.

Multimodal molecular imaging reveals high target uptake and specificity of ^{111}In and ^{68}Ga labeled fibrin-binding probes for thrombus detection in rats

Bruno L. Oliveira[1], **Francesco Blasi**[1], **Tyson A. Rietz**[1], **Nicholas J. Rotile**[1], **Helen Day**[1], and **Peter Caravan**[1,2]

[1]Athinoula A. Martinos Center for Biomedical Imaging, Department of Radiology, Massachusetts General Hospital, Harvard Medical School, Charlestown, MA, USA

[2]Institute for Innovation in Imaging, Massachusetts General Hospital, Boston, MA, USA

Abstract

We recently showed the high target specificity and favorable imaging properties of ^{64}Cu and Al^{18}F positron emission tomography (PET) probes for non-invasive imaging of thrombosis. Here, our aim was to evaluate new derivatives labeled with either with ^{68}Ga, ^{111}In, or ^{99m}Tc as thrombus imaging agents for PET and single-photon emission computed tomography (SPECT). In this study, the feasibility and potential of these probes for thrombus imaging was assessed in detail in two animal models of arterial thrombosis. The specificity of the probes was further evaluated using a triple-isotope approach with multimodal SPECT/PET/CT imaging.

Methods—Radiotracers were synthesized using a known fibrin-binding peptide conjugated to NODAGA, DOTA-MA, or a diethylenetriamine ligand (DETA-PA), followed by labeling with ^{68}Ga (FBP14, ^{68}Ga-NODAGA), ^{111}In (FBP15, ^{111}In-DOTA-MA) or ^{99m}Tc (FBP16, ^{99m}Tc(CO)$_3$-DETA-PA), respectively. PET or SPECT imaging, biodistribution, pharmacokinetics and metabolic stability were evaluated in rat models of mural and occlusive carotid artery thrombosis. In vivo target specificity was evaluated by comparing the distribution of the SPECT and PET probes with preformed ^{125}I-labeled thrombi and with a non-binding control probe using SPECT/PET/CT imaging.

Results—All three radiotracers showed similar affinity to soluble fibrin fragment DD(E) (K_i = 0.53–0.83 μM). After the kidneys, the highest uptake of ^{68}Ga-FBP14 and ^{111}In-FBP15 was in the thrombus (1.0 ± 0.2% ID/g) with low off-target accumulation. Both radiotracers underwent fast systemic elimination ($t_{1/2}$ = 8-15 min) through the kidneys, which led to highly conspicuous thrombi on PET and SPECT images. ^{99m}Tc-FBP16 displayed low target uptake and distribution consistent with aggregation and/or degradation. Triple isotope imaging experiments showed that both ^{68}Ga-FBP14 and ^{111}In-FBP15, but not the nonbinding derivative ^{64}Cu-D-Cys-FBP8, detected the location of the ^{125}I-labeled thrombus, confirming high target specificity.

Correspondence: Peter Caravan, 149 Thirteenth Street, Suite 2301, Charlestown, MA 02129, Phone: 617-643-0193, FAX: 617-726-7422, caravan@nmr.mgh.harvard.edu, First author: Bruno L Oliveira, 149 Thirteenth Street, Suite 2301, Charlestown, MA 02129, Phone: 617-643-0193, bljp2@cam.ac.uk.

Disclosures: Peter Caravan has equity in Factor 1A, LLC, the company holding the patent rights to the peptide used in this work.

Conclusion—^{68}Ga-FBP14 and ^{111}In-FBP15 have high fibrin affinity and thrombus specificity, and represent useful PET and SPECT probes for thrombus detection.

Keywords

Thrombosis; Fibrin; PET; SPECT

Introduction

Thrombosis is often the underlying cause of major cardiovascular diseases including stroke, myocardial infarction, deep vein thrombosis, and pulmonary embolism, which affect millions worldwide (1). Molecular targeting of coagulation factors (thrombin, Factor XIII, fibrinogen, fibrin) and activated platelets has shown high potential for thrombus imaging (2, 3). Particularly, fibrin is an ideal target for molecular imaging of thrombosis because its high specificity (present at high concentration in all clots but not in circulating blood) and high sensitivity (present in all thrombi whether arterial or venous, fresh or aged) of detection (4, 5). We previously reported feasibility of gadolinium-based fibrin-binding probes for thrombus imaging in both preclinical research (6-9) and clinical trials (10). Based on these results, we evaluated different peptides labeled with ^{64}Cu-DOTA as potential PET probes for thrombus imaging in animal models of thrombosis (11, 12). Choosing the best peptide from these initial studies, we then tested the effect of different chelators (CB-TE2A, NODAGA, NOTA-monoamide and Pycup) and isotopes (^{64}Cu and ^{18}F via aluminum fluoride complexation) on the in vivo properties of several probes for thrombus detection (13-15). The derivatives ^{64}Cu-FBP8 and Al^{18}F-FBP11 emerged as probes with high target to background ratios in PET imaging of thrombosis.

This structure-activity relationship suggested that other radiometals could be conjugated to the fibrin-specific peptide without loss of target affinity. ^{68}Ga is an attractive option for PET because of its short half-life and its availability from a FDA-approved generator (IDB Holland BV and Eckert & Ziegler), obviating the need for a cyclotron for isotope production (16). While PET offers superior resolution and absolute quantification, SPECT and scintigraphy are much more established in clinical practice due to lower costs and availability of many radioisotopes, namely ^{99m}Tc and ^{111}In (17, 18). Here, we evaluated three new fibrin-binding peptides radiolabeled with ^{68}Ga (FBP14), ^{111}In (FBP15) and ^{99m}Tc (FBP16) for thrombus imaging in two animal models. We used a mural thrombosis model to compare their target uptake, imaging efficacy, pharmacokinetic properties, and metabolic stability with our leading PET probe ^{64}Cu-FBP8. We also evaluated the radiotracers in a ferric chloride model of occlusive arterial thrombosis. ^{64}Cu-D-Cys-FBP8, a non-binding version of ^{64}Cu-FBP8 was employed as negative control. To further demonstrate specificity, we performed triple isotope SPECT/PET studies that combined a targeted probe, an untargeted control probe, and an ^{125}I-labeled-thrombus.

Materials and Methods

Additional information is reported in the supplemental material (available at http://jnm.snmjournals.org).

Synthesis and Affinity of the Fibrin-Binding Probes

The general synthetic route is depicted in Figure 1. The cyclic disulfide peptides L-Cys-Pep and D-Cys-Pep (Pep = FHC*HypY(3-Cl)DLCHIL-PXD, C* = L-Cys in L-Cys-Pep and D-Cys in D-Cys-Pep, Hyp = L-4-hydroxyproline, Y(3-Cl) = L-3-chlorotyrosine, PXD = para-xylenediamine) were prepared by solid phase peptide synthesis using Fmoc chemistry (14). ^{64}Cu-FBP8, ^{64}Cu-D-Cys-FBP8 and ^{68}Ga-FBP14 were synthesized by conjugation of L-Cys-Pep or D-Cys-Pep to ^{t}Bu-NOGAGA-NHS, followed by TFA hydrolysis and labeling with ^{64}Cu or ^{68}Ga. ^{111}In-FBP15 was synthesized by conjugation of the pre-activated DOTA chelator to L-Cys-Pep, and then by labeling with ^{111}In. ^{99m}Tc-FBP16 was obtained by coupling diethylenetriamine propanoic acid (DETA-PA) as the tetrafluorophenol ester to the active cyclic peptide, followed by hydrolysis of the Boc-protecting groups and labeling with $[^{99m}Tc(H_2O)_3(CO)_3]^+$. Reaction of the intermediates $(NODAGA)_2$Pep (Pep = L-Cys-Pep and D-Cys-Pep), $(DOTA\text{-}monoamide)_2$-L-Cys-Pep and $(DETA\text{-}PA)_2$-L-Cys-Pep with an excess of $^{nat}CuSO_4$, $^{nat}Ga(NO_3)_3$, $^{nat}InCl_3$ and $[^{nat}Re(CO)_3(H_2O)_3]Br$ (*nat* = naturally occurring isotope) resulted in the synthesis of the nonradioactive surrogates D-Cys-FBP8 (Cu), FBP14 (Ga), FBP15 (In), and FBP16 (Re). All intermediates and final compounds were purified by reversed phase high-performance liquid chromatography (HPLC) or using a Sep-Pak cartridge, and characterized by liquid chromatography-mass spectrometry (supplemental material). Chemical purities were >97%, determined by analytical HPLC analysis. Fibrin affinity of the nonradioactive surrogates was assessed as described in the supplemental material (12).

Animal Models and Probe Administration

All experiments were performed in accordance with the National Institutes of Health Guide for the Care and Use of Laboratory Animals, and were approved by the Institutional Animal Care and Use Committee at Massachusetts General Hospital. Adult male Sprague-Dawley rats (n = 36; 330-360 g, Charles River) were anesthetized with isoflurane (4% for induction, 2-2.5% for maintenance, in medical grade air) for all surgical procedures. The right femoral vein and artery were catheterized for probe injection and blood sampling, respectively. Mural thrombosis was induced by clamping of the common carotid artery for 5 minutes to prompt crush injury (12-15). Occlusive thrombosis was induced by ferric chloride (25% w/v in sterile saline) application on the common carotid artery (19). To detect the location of the thrombus with SPECT imaging, we prepared a pre-labeled clot by intracarotid microinjection of ^{125}I-fibrinogen (1 μL, 3-5 μCi) concomitant with the ferric chloride application. Fibrinogen (Calbiochem) was labeled with Na[^{125}I] (Perkin-Elmer) using Pierce™ iodination tubes (supplemental material).

Probes were injected 30 minutes after thrombus formation. Each rat was injected with 0.2-0.3 mCi for the PET probes or 0.9-1 mCi for the SPECT probes, in a volume of 0.4 mL followed by saline flush. This relatively high dose was to ensure that there was measurable radioactivity in the thrombosed and contralateral vessel, both of which weighed ca. 5 mg.

SPECT/PET Imaging and Analysis

SPECT/PET/CT scans were obtained with a dedicated small-animal multimodal scanner (Triumph; TriFoil Imaging). The SPECT camera is equipped with four detector heads and

converging five-pinhole collimators (pinhole diameter 2.5 mm). Instrument calibration was performed each day by scanning a phantom of known radioactivity. To evaluate the new fibrin-binding probes, rats with carotid crush injury were imaged for 60 minutes starting 30 minutes after the injection of the PET probes ^{64}Cu-D-cys-FBP8 (n = 2) and ^{68}Ga-FBP14 (n = 5) and the SPECT probes ^{111}In-FBP15 (n = 4) and ^{99m}Tc-FBP16 (n = 3) (protocol depicted in supplemental Figure 1). An additional cohort of rats (n = 3) were imaged for 90 minutes after the injection of ^{64}Cu-D-cys-FBP8, and then for an additional 90 minutes after injection of ^{64}Cu-FBP8. Target specificity was evaluated using a multimodal triple-isotope approach, where rats were first imaged by SPECT for 10 minutes to image the ^{125}I-labeled thrombus. Animals were then imaged for 30 minutes starting 30 minutes after injection of ^{111}In-FBP15, followed by 60 minutes of PET imaging after injection of either ^{68}Ga-FBP14 (n = 3) or ^{64}Cu-D-cys-FBP8 (n = 5) (supplemental Figure 1). The SPECT/PET field of view was 80 mm and approximately covered from the head to the base of the heart. For SPECT, ^{111}In photopeaks were set to 171 keV and 245 keV (± 15%) and scans were acquired for 225 seconds per projection and 16 projections per scan or for 100 seconds per projection and 16 projections per scan. The ^{125}I-thrombus was acquired for 38 seconds, 16 projections with an energy peak set to 35.5 keV (± 15%). After SPECT/PET acquisition, a CT scan was obtained with a constant infusion of iopamidol (Bracco, 0.4 mL/min) to increase contrast of the vessels. Images were acquired over 6 minutes with 512 projections with 2 frames per projection (exposure time per frame, 200 ms; peak tube voltage, 70 kV; tube current, 177 mA).

SPECT, PET and CT images were reconstructed using the LabPET and the X-SPECT softwares (TriFoil Imaging) to a voxel size of 0.5×0.5×0.6 mm^3 (PET), 1.3×1.3×0.9 mm^3 (SPECT), and isotropic 0.3 mm^3 (CT). Data of each frame were reconstructed using a maximum-likelihood expectation maximization algorithm with 30 iterations. SPECT images were reconstructed using an ordered subset expectation maximization algorithm with five iterations of four subsets. All images were corrected for decay, randoms, and dead time; CT data were used to provide for attenuation correction. Reconstructed data were quantitatively evaluated using AMIDE. Volumes of interest (VOIs) were drawn on fused, co-registered images to localize the hot spot at the site of the injured common carotid artery (4.2 mm^3), and background tissues including muscle (acromiotrapezius, 25 mm^3), heart (25 mm^3), and contralateral artery (4.2 mm^3). Results were expressed as percentage injected dose/cubic centimeter of tissue (% ID/cc).

Ex vivo analysis

Animals were euthanized at the end of the imaging session, and tissues were harvested and processed for biodistribution, autoradiography, metabolic stability, and functional fibrin-binding assay. Serial blood samples were collected at 0, 2, 5, 10, 15, 30, 60, 120, and 180 minutes in ethylenediaminetetraacetic acid tubes and the radioactivity measured with a gamma-counter (CobraII Auto-Gamma; Packard) to assess clearance of total radioactivity. To measure the amount of functional probe, plasma samples were checked for fibrin binding by incubation with immobilized fibrin (supplemental material). To evaluate plasma stability, samples collected at 2, 15, 30, and 60 minutes post-injection were analyzed by HPLC (supplemental material). Blood half-lives were calculated from a biexponential fit to the

clearance data of the functional radiotracers. For the biodistribution studies, animals were euthanized at 120 or 180 minutes after injection. The tissues were weighed (thrombus, contralateral carotid artery, blood, chest, abdominal organs, brain, rectus femoris muscle, femur bone), and radioactivity in each tissue was measured to determine the percentage of injected dose per gram of tissue (% ID/g). Thrombosed and contralateral carotid arteries were further analyzed by autoradiography using a multipurpose film with a Cyclone Plus Phosphor system and quantified using OptiQuant 5.0 software (Perkin-Elmer) to obtain raw values expressed as digital light units/mm^2. To increase the power of the biodistribution study, additional rats with crush injury were characterized by biodistribution and autoradiography but not PET: ^{64}Cu-D-cys-FBP8 (n = 5 total), ^{111}In-FBP15 (n = 8 total), and ^{99m}Tc-FBP16 (n = 6 total).

Statistics

Data were expressed as mean ± SEM. Differences between groups were compared using ANOVA followed by Bonferroni post hoc test. A $P < 0.05$ was considered significant.

Results

Chemistry, radiochemistry, and affinity of the fibrin-binding probes

^{64}Cu-FBP8 and ^{64}Cu-D-Cys-FBP8 were obtained by reaction of the precursors $(NODAGA)_2$-L-Cys-Pep and $(NODAGA)_2$-D-Cys-Pep with $^{64}CuCl_2$ (30 minutes at 60 °C), in yields >99% as assessed by radio-HPLC with specific activities of 0.35-0.71 mCi/nmol. For radiolabeling of ^{68}Ga-FBP14, ^{68}Ga was eluted with 0.6M HCl from a 50 mCi ^{68}Ge/^{68}Ga generator (iThemba/IDB Holland BV), buffered with sodium acetate and reacted with $(NODAGA)_2$-L-Cys-Pep (20 minutes at 60 °C), obtaining quantitative yield by radio-HPLC and specific activities of 0.26-0.35 mCi/nmol. Any ^{68}Ge breakthrough was removed by Sep-Pak C18 purification. ^{111}In-FBP15 was obtained in 90-95% yield by reacting $^{111}InCl_3$ with $(DOTA\text{-}MA)_2$-L-Cys-Pep (45 minutes at 85 °C) to give specific activities of 0.18-0.23 mCi/nmol, following Sep-Pak purification to remove free ^{111}In. Reaction of the peptide conjugate $(DETA\text{-}PA)_2$-L-Cys-Pep with the precursor *fac*-$[^{99m}Tc(CO)_3(H_2O)_3]^+$ gave ^{99m}Tc-FBP16 (30 minutes at 100 °C), with specific activities of 0.10-0.12 mCi/nmol. The reaction was monitored by radio-HPLC and iTLC, which showed >99% conversion to the radiolabeled peptide, with no need of purification. The nonradioactive surrogates were obtained by reaction of the intermediate ligands with an excess of metal ion ($^{nat}CuSO_4$, $^{nat}Ga(NO_3)_3$, $^{nat}InCl_3$ and $[^{nat}Re(H_2O)_3(CO)_3]Br$), followed by Sep-Pak or preparative HPLC purification (purity >98%). ^{68}Ga-FBP14, ^{111}In-FBP15, and ^{99m}Tc-FBP16 displayed similar affinity to the fibrin fragment DD(E) (0.53–0.83 μM, supplemental Table 1), comparable to that of the MR probe EP-2104R (0.31-0.35 μM). The non-binding probe ^{64}Cu-D-Cys-FBP8 showed no displacement of the fluorescent probe in this assay and we estimate fibrin affinity >1000 μM.

In vivo evaluation of ^{68}Ga-FBP14, ^{111}In-FBP15 and ^{99m}Tc-FBP16

The radiolabeled peptides were evaluated by SPECT and PET imaging according to the scheme depicted in Figure 2. Both ^{68}Ga-FBP14 and ^{111}In-FBP15, but not ^{99m}Tc-FBP16, revealed the thrombus as a region of high radioactivity in PET and SPECT, respectively.

Quantification showed a significantly higher radioactivity in the thrombus compared with the background tissues. In particular, there was a >4-fold difference between the thrombus and contralateral carotid artery.

These findings were confirmed by ex vivo gamma-counting of the harvested tissues (Figure 3). ^{68}Ga-FBP14 and ^{111}In-FBP15 accumulated 3-4 times more in the thrombosed carotid than in the contralateral vessel (supplemental Table 2 and supplemental Figure 2). The thrombus was the tissue with the second highest uptake (1% ID/g) after the kidneys (2-4% ID/g), while little radioactivity was detected in the liver (0.2-0.3% ID/g). ^{99m}Tc-FBP16, however, showed a low thrombus-to-contralateral vessel ratio but high liver (3.2% ID/g), lung (1.5% ID/g) and spleen (1.9% ID/g) accumulation, suggestive of aggregation in vivo. Autoradiographs of the excised carotids showed increased tracer accumulation at the thrombus site for rats injected with ^{68}Ga-FBP14 and ^{111}In-FBP15 but not with ^{99m}Tc-FBP16 (Figure 3B). Serial blood draws taken from 0 to 120 minutes post-injection (p.i.) indicated that the radioactivity cleared quickly for ^{68}Ga-FBP14 and ^{111}In-FBP15 but not with ^{99m}Tc-FBP16, which showed residual radioactivity persisting in the blood even after 120 minutes (Figure 3C). The estimated blood half-life derived from bi-exponential fitting of the intact radiotracers was 8.0 ± 3.1, 14.6 ± 5.6 and 5.9 ± 16.2 minutes for ^{68}Ga-FBP14, ^{111}In-FBP15 and ^{99m}Tc-FBP16, respectively.

HPLC analysis of blood plasma sampled at different time points after injection of ^{68}Ga-FBP14 and ^{111}In-FBP15 indicated that at 1 hour post-injection ∼60% of the plasma radioactivity was intact probe (supplemental Figure 3). The remaining ∼40% were traced to transmetalation of ^{68}Ga and ^{111}In from the probes to plasma proteins.

In vivo target specificity of ^{68}Ga-FBP14 and ^{111}In-FBP15

We aimed to demonstrate in vivo that our thrombus imaging agents actually target fibrin, and that the specificity of the probes strictly depends on the fibrin-targeting properties of the peptide. To confirm specificity for fibrin we first injected the non-binding probe ^{64}Cu-D-Cys-FBP8 in rats after mural carotid thrombosis. This probe is identical to ^{64}Cu-FBP8 except that one of the cysteines has its chirality inverted which abrogates fibrin binding (20). PET imaging showed no uptake in the thrombus (Figure 4A). Similarly, PET quantification and autoradiography did not show significant differences in uptake between thrombosed and contralateral carotid arteries (Figure 4B). Ex vivo biodistribution (supplemental Figure 4) confirmed the imaging results. We performed an additional validation by continuously imaging rats injected first with ^{64}Cu-D-Cys-FBP8 and then with ^{64}Cu-FBP8. PET imaging did not show uptake of ^{64}Cu-D-Cys-FBP8 in the thrombosed carotid artery but after ^{64}Cu-FBP8 administration a hot spot was clearly visible (Figure 4C). Time-radioactivity curves showed comparable uptake between ipsilateral and contralateral vessels after injection of ^{64}Cu-D-Cys-FBP8, but a significant difference after injection of ^{64}Cu-FBP8. Analysis of blood samples collected over the course of the study confirmed that ^{64}Cu-D-Cys-FBP8 does not bind to fibrin whereas ^{64}Cu-FBP8 has high target binding (Figure 4D).

Having validated the inactive probe, we designed a multimodal, multi-isotope imaging experiment to further confirm the high target specificity of the probes to fibrin (Figure 5). We first formed a radioactive thrombus by injecting ^{125}I-fibrinogen into an isolated section

of the common carotid artery followed by application of ferric chloride to initiate thrombosis. ^{125}I-fibrinogen was radiolabeled using the iodogen technique (yield = 94.3 ± 3.8%) and showed clotting activity >90% (supplemental material). SPECT imaging of ^{125}I-thrombus bearing rats revealed the presence of a hot spot localized to the thrombosed carotid artery (supplemental Figure 5). ^{125}I-thrombus bearing rats were then systemically injected with ^{111}In-FBP15 and finally with ^{68}Ga-FBP14 (Figure 5A). The presence of an isolated region of high uptake was detected with both SPECT and PET on the thrombosed common carotid artery, with co-localization of ^{125}I, ^{111}In and ^{68}Ga radioactivities. To rule out SPECT/PET radioactivity spillover, one ^{125}I-thrombus bearing rat underwent PET imaging after the injection of ^{111}In-FBP15 but before ^{68}Ga-FBP14 administration (supplemental Figure 6). In a second study, ^{125}I-thrombus bearing rats were injected with ^{111}In-FBP15 and then with ^{64}Cu-D-Cys-FBP8. SPECT imaging showed co-localization between ^{125}I and ^{111}In radioactivities, but PET imaging did not reveal significant uptake at the target site (Figure 5B).

Ex vivo biodistribution confirmed the high uptake of ^{111}In-FBP15 in the thrombus (supplemental Figure 7). At 180-minutes post-injection, the thrombus had the highest uptake (0.94% ID/g) just after kidney (2.0% ID/g), with high thrombus-to-background ratios.

Discussion

We recently screened several fibrin-targeted probes comprising a fibrin-specific peptide conjugated to a chelator labeled with either ^{64}Cu or Al^{18}F for thrombus imaging (12-15). In the present work, we extend our findings to other clinically useful isotopes, ^{68}Ga, ^{111}In and ^{99m}Tc, for both PET and SPECT to facilitate bench-to-bedside translation. ^{68}Ga has significant commercial potential and is a convenient alternative to the cyclotron-produced PET isotopes ^{68}Cu and ^{18}F because it can be eluted from a ^{68}Ge/^{68}Ga generator on site. SPECT still has a larger installed base of cameras and lower cost than PET, and widespread availability of generator produced ^{99m}Tc, as well as ^{111}In (17, 18). NODAGA for ^{64}Cu and ^{68}Ga, DOTA-MA for ^{111}In and the diethylenetriamine for "^{99m}Tc(CO)$_3$" were chosen as chelators because they form highly stable complexes with these metal ions (21, 22). Imaging studies showed that the thrombus target was clearly visualized by ^{68}Ga-FBP14 and ^{111}In-FBP15 in two different animal models with high thrombus-to-background ratios, but that ^{99m}Tc-FBP16 was ineffective. Ex vivo studies biodistribution confirmed that ^{68}Ga-FBP14 and ^{111}In-FBP15 exhibited low uptake in most nontarget tissues. Only the kidneys retained more radioactivity than the thrombosed artery. Finally, biodistribution studies demonstrated that ^{99m}Tc-FBP16 is not effective for detection of thrombus due to high liver, lung and spleen accumulation, consistent with colloidal aggregation in vivo.

Recently it was reported that ^{111}In-labeled fibrin-binding peptide EPep, containing the same peptide used in EP-2104R and closely related to the peptide used here, was evaluated in rat model of thrombosis. Both ^{111}In-EPep and ^{111}In-FBP15 have high thrombus uptake (0.74% ID/g at 4h p.i. vs. 1.04% ID/g at 3h p.i., respectively) and comparable accumulation in non-target organs, including liver (^{111}In-EPep, ∼0.1% ID/g at 4h p.i. vs. 0.23% ID/g for ^{111}In-FBP15 at 3h p.i.) and kidney (^{111}In-EPep ∼1.6% ID/g at 4h p.i. vs. 2.0% ID/g for ^{111}In-

FBP15 at 3h p.i.). The similar distribution profile of both probes may be expected since both are derivatives of EP-2104R (12, 23).

The rapid blood clearance and low retention in most organs suggest translational potential for ^{68}Ga-FBP14 and ^{111}In-FBP15 as thrombus imaging agents. Compared to our previous fibrin-binding probes, ^{68}Ga-FBP14 and ^{111}In-FBP15 are less stable in vivo (∼60% of probe intact at 1h p.i. compared to >95% intact for ^{64}Cu-FBP8), which resulted in higher radioactivity in the blood and contralateral carotid. Nevertheless, the relatively high clot uptake, combined with the lower kidney retention, suggest that these probes are still promising for clinical applications. ^{64}Cu-FBP8 was recently reported to have favorable dosimetry properties for human translation, (24) and this should be true of ^{68}Ga-FBP14 as well owing to the shorter half-life of ^{68}Ga compared to ^{64}Cu.

Binding specificity is frequently evaluated in vivo by showing that co-injection of a large molar excess of free ligand blocks the binding of the probe to its target. Fibrin is derived from circulating fibrinogen present at 2–4 g/L (6-12 μM) in plasma and, upon clotting, the concentration of polymerized monomer is 10s to 100s of μM. Therefore, blocking studies are limited by the excessive amount of unlabeled peptide needed to inhibit binding. Instead, we used a multimodal triple-isotope imaging approach. Using an ^{125}I-labeled thrombus and the nontargeted derivative ^{64}Cu-D-Cys-FBP8, we proved by SPECT/PET imaging that ^{68}Ga-FBP14 and ^{111}In-FBP15 detect thrombus by directly targeting fibrin. First, we performed a negative control experiment with ^{64}Cu-D-Cys-FBP8, which shares all the features of the parent probe ^{64}Cu-FBP8 except the chirality of one of the cysteines. *In vitro* assays with the soluble fibrin fragment DD(E) revealed that the active compounds have similar sub-micromolar affinity for fibrin (K_i = 0.53-0.83 μM) as opposed to ^{64}Cu-D-Cys-FBP8 (K_i >1000 μM). Moreover, PET imaging in crush-injured rats showed that ^{64}Cu-D-Cys-FBP8 could not distinguish the injured carotid from the surrounding tissues; conversely after sequential administration of ^{64}Cu-FBP8 a clear hot spot was detected at the level of the thrombosed carotid. We then showed that systemically administered ^{111}In-FBP15 colocalized with a pre-formed ^{125}I-labeled thrombus, whereas the untargeted ^{64}Cu-D-Cys-FBP8 did not. We further showed that both ^{68}Ga-FBP14 and ^{111}In-FBP15 colocalize with the ^{125}I-labeled clot.

Optical imaging/microscopy routinely makes use of multiple fluorophores to localize a probe to a specific cell type or organelle. Multielement SPECT and/or combined SPECT-PET offer the potential for analogous in vivo validation. To date, a limited number of studies have shown the utility of multi-isotopes imaging in the design and validation of new molecular imaging tracers (25-27). A challenge in multielement SPECT is overlap in the emission spectra of the two respective radionuclides as well as crosstalk contamination resulting in the need for complex software algorithms to compensate for these effects. Acquisition of SPECT and PET scans with multiple radionuclides is also limited by SPECT “contamination” from down-scattered 511 keV photons and attenuation of the PET coincident photons by the SPECT collimators (25). However with a careful choice of the radionuclides and using a sequential imaging protocol, dual SPECT/PET studies hold great potential for radiopharmaceutical development by allowing the acquisition of additional/complementary information about an in vivo target using multi tracers in the same animal.

Conclusion

We identified 2 novel PET and SPECT probes for detection of thrombosis with high fibrin affinity and favorable imaging properties in two rat models of arterial thrombosis. The rapid blood clearance and low off-target retention suggest translational potential for ^{68}Ga-FBP14 and ^{111}In-FBP15 as thrombus imaging agents.

Supplementary Material

Refer to Web version on PubMed Central for supplementary material.

Acknowledgments

This work was supported by HL109448 from the National Heart, Lung, and Blood Institute. The small-animal SPECT/PET/CT system was funded by RR029495 from the National Center for Research Resources.

Financial support: HL109448 (National Heart, Lung, and Blood Institute), RR029495 (National Center for Research Resources)

References

1. Go AS, Mozaffarian D, Roger VL, et al. Executive Summary: Heart Disease and Stroke Statistics-2014 Update A Report From the American Heart Association. Circulation. 2014; 129:399–410. [PubMed: 24446411]
2. de Haas HJ, Narula J, Fuster V. From molecular imaging to pathogenesis and vice versa. Circulation-Cardiovascular Imaging. 2014; 7:581–585. [PubMed: 25027453]
3. Houshmand S, Salavati A, Hess S, Ravina M, Alavi A. The role of molecular imaging in diagnosis of deep vein thrombosis. Am J Nucl Med Mol Imaging. 2014; 4:406–425. [PubMed: 25143860]
4. Ciesienski K, Caravan P. Molecular MRI of thrombosis. Curr Cardiovasc Imaging Rep. 2011; 4:77–84. [PubMed: 21253438]
5. Undas A, Ariens RAS. Fibrin clot structure and function a role in the pathophysiology of arterial and venous thromboembolic diseases. Arteriosclerosis Thrombosis and Vascular Biology. 2011; 31:E88–E99.
6. Nair SA, Kolodziej AF, Bhole G, Greenfield MT, McMurry TJ, Caravan P. Monovalent and bivalent fibrin-specific MRI contrast agents for detection of thrombus. Angew Chem Int Ed. 2008; 47:4918–4921.
7. Overoye-Chan K, Koerner S, Looby RJ, et al. EP-2104R: a fibrin-specific gadolinium-Based MRI contrast agent for detection of thrombus. J Am Chem Soc. 2008; 130:6025–6039. [PubMed: 18393503]
8. Uppal R, Ay I, Dai G, Kim YR, Sorensen AG, Caravan P. Molecular MRI of intracranial thrombus in a rat ischemic stroke model. Stroke. 2010; 41:1271–1277. [PubMed: 20395615]
9. Loving GS, Caravan P. Activation and retention: a magnetic resonance probe for the detection of acute thrombosis. Angew Chem Int Ed. 2014; 53:1140–1143.
10. Vymazal J, Spuentrup E, Cardenas-Molina G, et al. Thrombus imaging with fibrin-specific gadolinium-based MR contrast agent EP-2104R results of a Phase II clinical study of feasibility. Invest Radiol. 2009; 44:697–704. [PubMed: 19809344]
11. Uppal R, Catana C, Ay I, Benner T, Sorensen AG, Caravan P. Bimodal thrombus imaging: simultaneous PET/MR imaging with a fibrin-targeted dual PET/MR probe-feasibility study in rat model. Radiology. 2011; 258:812–820. [PubMed: 21177389]
12. Ciesienski KL, Yang Y, Ay I, et al. Fibrin-targeted PET probes for the detection of thrombi. Mol Pharm. 2013; 10:1100–1110. [PubMed: 23327109]

13. Ay I, Blasi F, Rietz TA, et al. In vivo molecular imaging of thrombosis and thrombolysis using a fibrin-binding positron emission tomographic probe. Circ Cardiovasc Imaging. 2014; 7:697–705. [PubMed: 24777937]
14. Blasi F, Oliveira BL, Rietz TA, et al. Effect of chelate type and radioisotope on the imaging efficacy of 4 fibrin-specific PET probes. J Nucl Med. 2014; 55:1157–1163. [PubMed: 24790217]
15. Boros E, Rybak-Akimova E, Holland JP, et al. Pycup--a bifunctional, cage-like ligand for (64)Cu radiolabeling. Mol Pharmaceutics. 2014; 11:617–629.
16. Fani M, Andre JP, Maecke HR. 68Ga-PET: a powerful generator-based alternative to cyclotron-based PET radiopharmaceuticals. Contrast Media Mol Imaging. 2008; 3:67–77. [PubMed: 18383558]
17. Pimlott SL, Sutherland A. Molecular tracers for the PET and SPECT imaging of disease. Chem Soc Rev. 2011; 40:149–162. [PubMed: 20818455]
18. Rahmim A, Zaidi H. PET versus SPECT: strengths, limitations and challenges. Nucl Med Commun. 2008; 29:193–207. [PubMed: 18349789]
19. Kurz KD, Main BW, Sandusky GE. RAT MODEL OF ARTERIAL THROMBOSIS INDUCED BY FERRIC-CHLORIDE. Thrombosis Research. 1990; 60:269–280. [PubMed: 2087688]
20. Kolodziej AF, Zhang Z, Overoye-Chan K, Jacques V, Caravan P. Peptide optimization and conjugation strategies in the development of molecularly targeted magnetic resonance imaging contrast agents. Methods Mol Biol. 2014; 1088:185–211. [PubMed: 24146405]
21. Lane SR, Veerendra B, Rold TL, et al. (99)mTc(CO)(3)-DTMA bombesin conjugates having high affinity for the GRP receptor. Nucl Med Biol. 2008; 35:263–272. [PubMed: 18355681]
22. Wadas TJ, Wong EH, Weisman GR, Anderson CJ. Coordinating radiometals of copper, gallium, indium, yttrium, and zirconium for PET and SPECT imaging of disease. Chem Rev. 2010; 110:2858–2902. [PubMed: 20415480]
23. Starmans LWE, van Duijnhoven SMJ, Rossin R, et al. Evaluation of In-111-labeled EPep and FibPep as tracers for fibrin SPECT imaging. Mol Pharm. 2013; 10:4309–4321. [PubMed: 24099178]
24. Blasi F, Oliveira BL, Rietz TA, et al. Radiation dosimetry of the fibrin-binding probe 64Cu-FBP8 and its feasibility for PET imaging of deep vein thrombosis and pulmonary embolism in rats. J Nucl Med. 2015; 56:1088–1093. [PubMed: 25977464]
25. Fakhri GE. Ready for prime time? Dual tracer PET and SPECT imaging. Am J Nucl Med Mol Imaging. 2012; 2:415–417. [PubMed: 23145358]
26. Hijnen NM, de Vries A, Nicolay K, Grull H. Dual-isotope 111In/177Lu SPECT imaging as a tool in molecular imaging tracer design. Contrast Media Mol Imaging. 2012; 7:214–222. [PubMed: 22434634]
27. Hueting R, Kersemans V, Tredwell M, et al. A dual radiolabelling approach for tracking metal complexes: investigating the speciation of copper bis(thiosemicarbazonates) in vitro and in vivo. Metallomics. 2015; 7:795–804. [PubMed: 25768310]

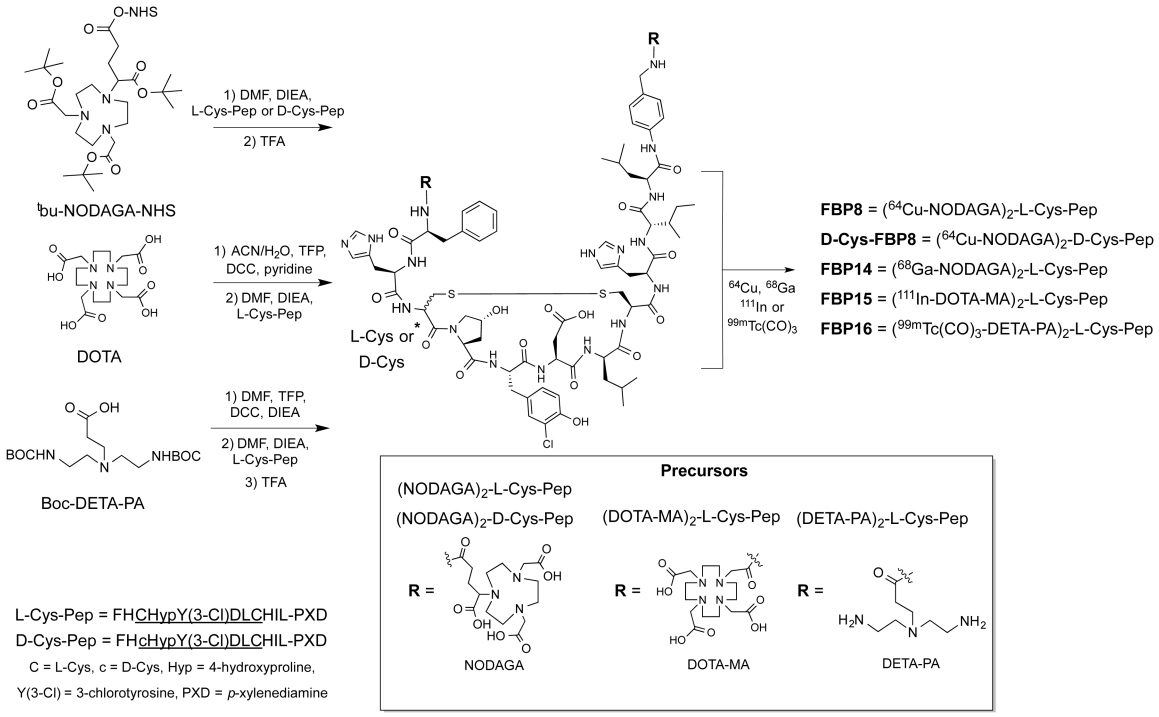

Figure 1.
Synthesis of the fibrin-binding probes.

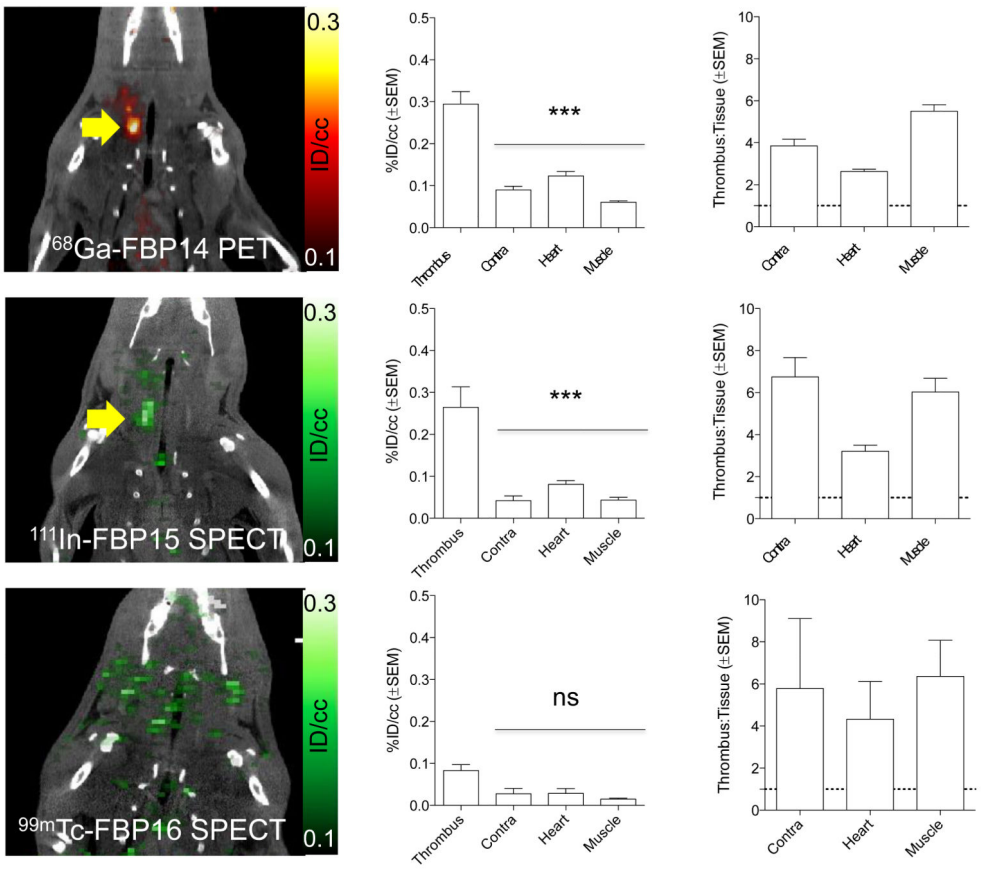

Figure 2.

Representative PET and SPECT images (crush model, 30-90 min p.i.) showing persistent thrombus signal (arrow) after injection of ^{68}Ga-FBP14 (n = 5) and ^{111}In-FBP15 (n = 4), but not for ^{99m}Tc-FP16 (n = 3). PET and SPECT quantification revealed high target radioactivity for ^{68}Ga-FBP14 and ^{111}In-FBP15 compared with background tissues, resulting in high thrombus-to-background radioactivity ratios. ***P <0.001.

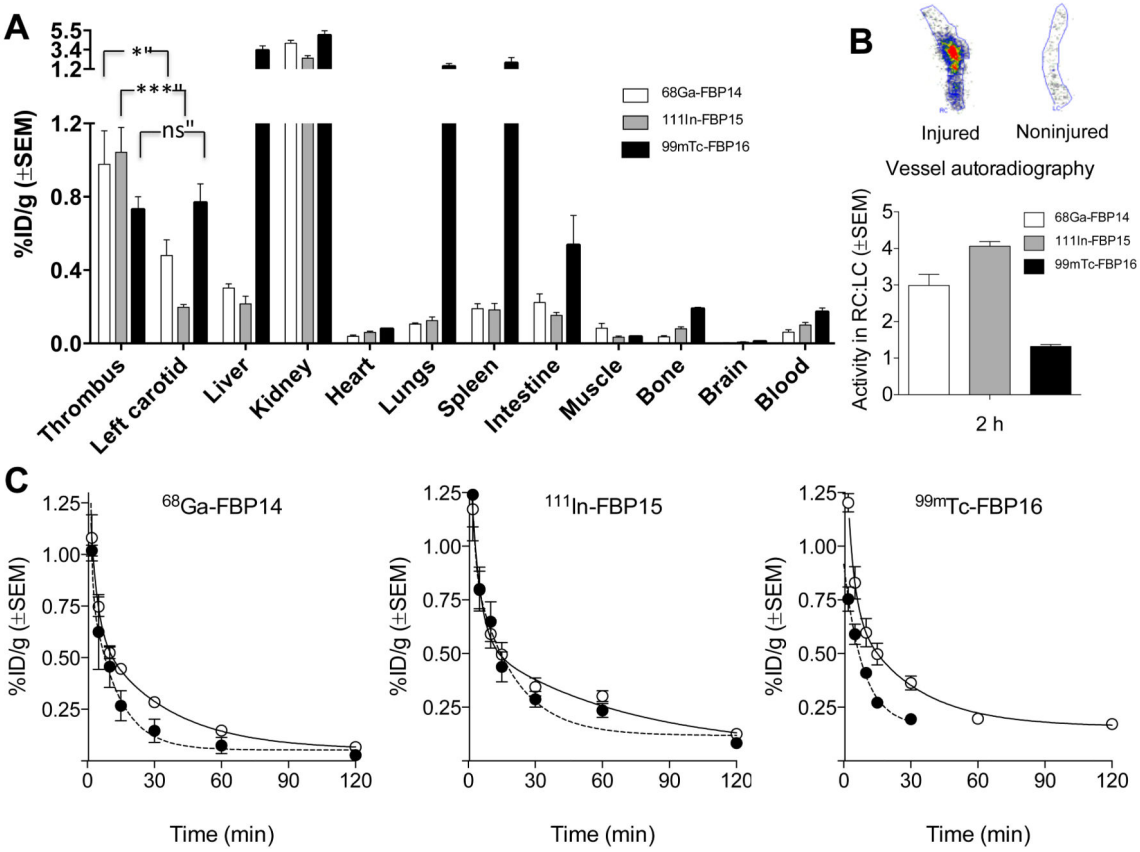

Figure 3.

(A) Biodistribution at 120 minutes (crush model; ^{68}Ga-FBP14, n = 5; ^{111}In-FBP15, n = 8; ^{99m}Tc-FBP16, n = 6). (B) Representative autoradiographs of excised injured and contralateral carotid arteries after injection of ^{111}In-FBP15, and ipsilateral:contralateral ratios for each probe (n = 5 – 6 per probe). (C) Pharmacokinetic data from ex vivo blood analyses (^{68}Ga-FBP14, n = 5; ^{111}In-FBP15, n = 8; ^{99m}Tc-FBP16, n = 4; ○ total radioactivity in plasma; ● functional probe). *P <0.05. ***P <0.001.

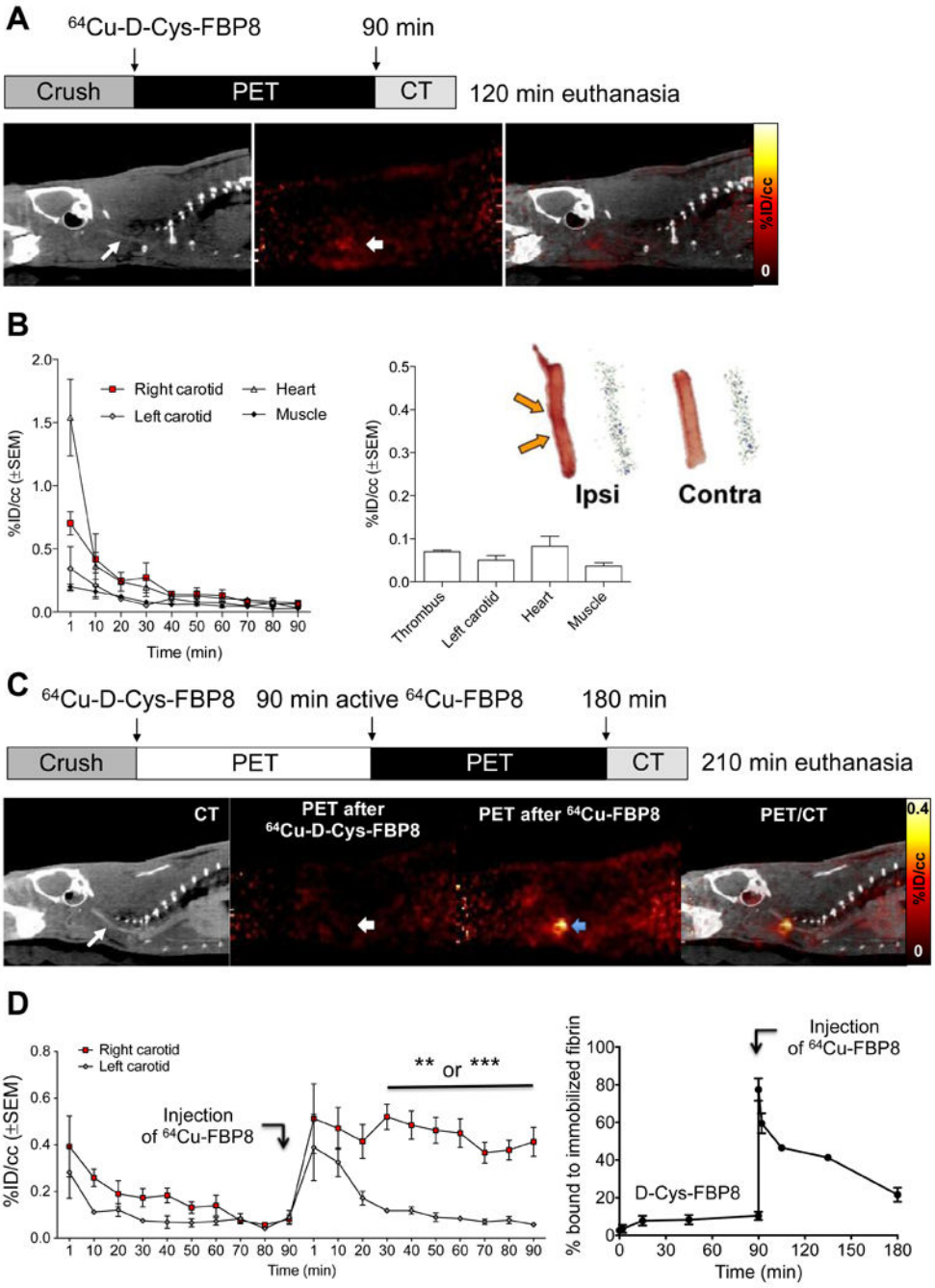

Figure 4.

(A) CT, PET, and fused images from an animal injected with ^{64}Cu-D-Cys-FBP8 after carotid crush injury (n = 2). Contrast-enhanced CT angiography was used to detect the common carotid artery (thin arrow). The thrombus location could not be detected by PET. (B) Time–radioactivity curves obtained from PET imaging, mean radioactivity values (30 - 90 min p.i.), and representative photograph and autoradiograph of ipsilateral and contralateral carotid arteries showing comparable radioactivity levels between thrombus and background. (C) PET-CT imaging (n = 3) after sequential injection of ^{64}Cu-D-Cys-FBP8,

followed by injection of its active analogue ^{64}Cu-FBP8. Thrombus uptake was only detected after injection of ^{64}Cu-FBP8 (blue arrow). (D) Statistically significant difference in thrombus versus contralateral artery uptake for ^{64}Cu-FBP8 but not ^{64}Cu-D-Cys-FBP8. *In vitro* binding studies of blood plasma incubated with immobilized fibrin showed significantly lower binding for ^{64}Cu-D-Cys-FBP8 in comparison to ^{64}Cu-FBP8 (n = 2). **P <0.01.

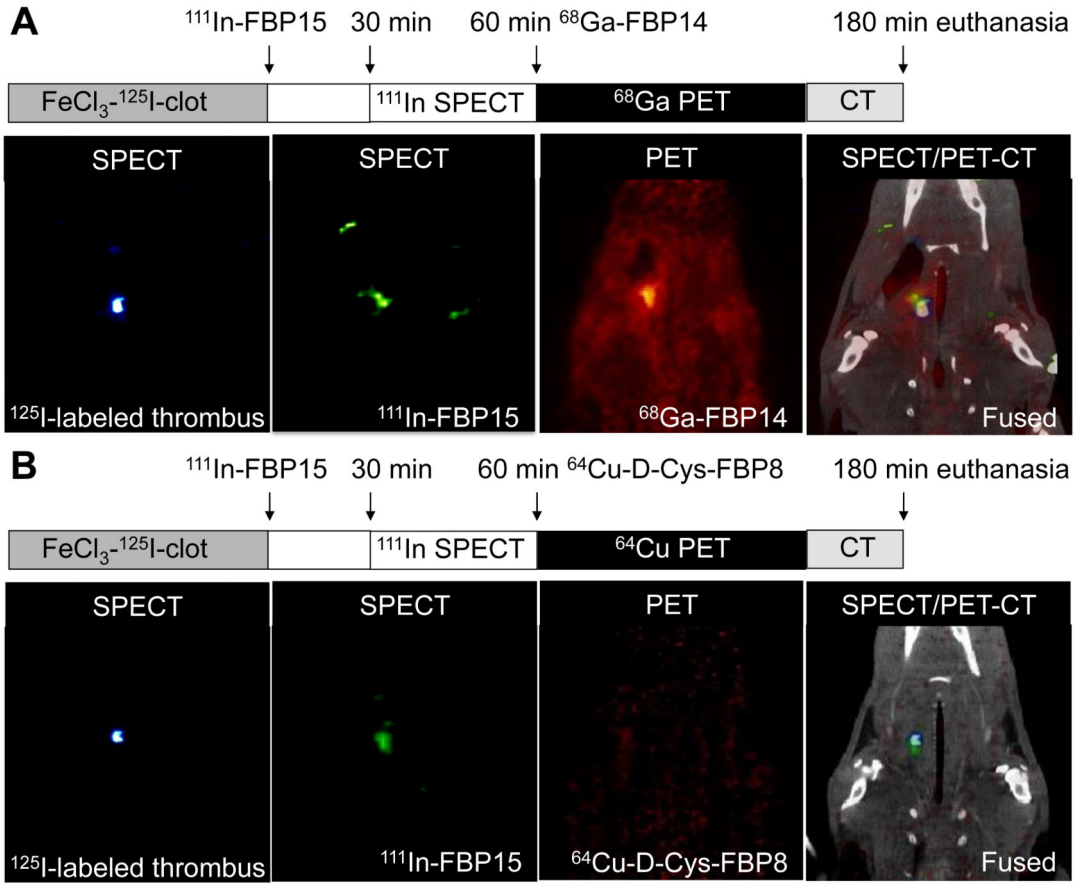

Figure 5.

Triple-isotope SPECT/PET-CT studies in ^{125}I-thrombus bearing rats. (A) From left to right: 35 keV SPECT image showing ^{125}I-labeled thrombus; 171 - 245 keV SPECT imaging after ^{111}In-FBP15 injection showing high uptake in region of the thrombus; PET image after ^{68}Ga-FBP14 injection showing focal signal intensity in the region of the carotid artery; fused SPECT/PET-CT images showing that ^{111}In-FBP15 and ^{68}Ga-FBP14 colocalize to ^{125}I-labeled thrombus. (B) From left to right: 35 keV SPECT image showing ^{125}I-labeled thrombus; 171 - 245 keV SPECT imaging after ^{111}In-FBP15 injection showing high uptake in region of the thrombus; PET image after ^{64}Cu-D-Cys-FBP8 injection shows low signal intensity in the field of view; fused SPECT/PET-CT images show that fibrin-targeted ^{111}In-FBP15 but not non-specific ^{64}Cu-D-Cys-FBP8 colocalizes to the ^{125}I-labeled thrombus.